

This is a repository copy of *Inverse Isotope Effects in Single-Crystal to Single-Crystal Reactivity and the Isolation of a Rhodium Cyclooctane  $\sigma$ -Alkane Complex*.

White Rose Research Online URL for this paper:

<https://eprints.whiterose.ac.uk/id/eprint/182529/>

Version: Accepted Version

---

**Article:**

Doyle, Laurence Robertson, Galpin, Martin R., Furfari, Sam et al. (7 more authors) (2022) Inverse Isotope Effects in Single-Crystal to Single-Crystal Reactivity and the Isolation of a Rhodium Cyclooctane  $\sigma$ -Alkane Complex. *Organometallics*. pp. 284-292. ISSN: 0276-7333

<https://doi.org/10.1021/acs.organomet.1c00639>

---

**Reuse**

Items deposited in White Rose Research Online are protected by copyright, with all rights reserved unless indicated otherwise. They may be downloaded and/or printed for private study, or other acts as permitted by national copyright laws. The publisher or other rights holders may allow further reproduction and re-use of the full text version. This is indicated by the licence information on the White Rose Research Online record for the item.

**Takedown**

If you consider content in White Rose Research Online to be in breach of UK law, please notify us by emailing [eprints@whiterose.ac.uk](mailto:eprints@whiterose.ac.uk) including the URL of the record and the reason for the withdrawal request.

# Inverse Isotope Effects in Single-Crystal to Single-Crystal Reactivity and the Isolation of a Rhodium Cyclooctane $\sigma$ -Alkane Complex.

Laurence R. Doyle,<sup>\*,[a]</sup> Martin R. Galpin,<sup>[b]</sup> Samantha K. Furfari,<sup>[a]</sup> Bengt E. Tegner,<sup>[c]</sup> Antonio J. Martínez-Martínez,<sup>[d]†</sup> Adrian C. Whitwood,<sup>[a]</sup> Scott A. Hicks,<sup>[a]</sup> Guy C. Lloyd-Jones,<sup>[c]</sup> Stuart A. Macgregor,<sup>\*,[c]</sup> and Andrew S. Weller<sup>\*,[a]</sup>

[a] Department of Chemistry, University of York, Heslington, York, YO10 5DD (UK); [b] Physical and Theoretical Chemistry Laboratories, University of Oxford, Oxford, OX1 3QZ (UK); [c] School of Chemical Sciences, Heriot-Watt University, Edinburgh, Scotland, EH14, 4AS (UK); [d] Department of Chemistry, Mansfield Road, University of Oxford, Oxford, OX1 3TA (UK); [e] Department of Chemistry, University of Edinburgh, Edinburgh, Scotland, EH9 3FJ (UK).

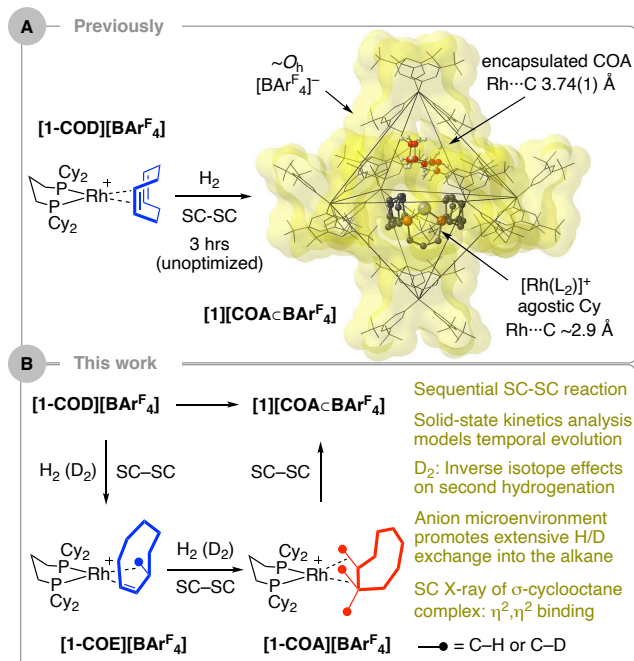
The sequential solid-gas single-crystal to single-crystal reaction of  $[\text{Rh}(\text{Cy}_2\text{P}(\text{CH}_2)_3\text{PCy}_2)(\text{COD})][\text{BAR}^{\text{F}}_4]$  with  $\text{H}_2$  or  $\text{D}_2$  was followed by in situ  $^{31}\text{P}\{^1\text{H}\}$  SSNMR, and ex-situ by solution quenching and GC-MS. This was quantified using a two-step Johnson-Mehl-Avrami-Kolgoromov (JMAK) model, that revealed an inverse isotope effect for the second addition of  $\text{H}_2$ , that forms a  $\sigma$ -alkane complex  $[\text{Rh}(\text{Cy}_2\text{P}(\text{CH}_2)_3\text{PCy}_2)(\text{COA})][\text{BAR}^{\text{F}}_4]$ . Using  $\text{D}_2$ , a temporal window is determined in which a structural solution for this  $\sigma$ -alkane complex is possible, which reveals an  $\eta^2, \eta^2$ -binding mode to the Rh(I) center, as supported by periodic DFT calculations. Extensive H/D exchange occurs during addition of  $\text{D}_2$ , as promoted by the solid-state microenvironment.

## INTRODUCTION

The isotopic substitution of hydrogen for deuterium is an invaluable tool for the study of mechanism in synthesis and catalysis.<sup>1-3</sup> Zero-point energy differences of E–H/D bonds (e.g., C–H/D) lead to changes in the temporal evolution of a reaction manifold if E–H bond activation, or formation, occurs at or before the rate-controlling step. This can be associated with a single transition-state (a kinetic isotope effect, KIE), or preceding equilibria that result in a composite KIE (equilibrium isotope effect, EIE). While KIE or EIE normally act to slow the overall progress of a reaction when using the heavier isotopologue, an acceleration reflects an inverse isotope effect.<sup>4</sup> While not always straightforward,<sup>5,6</sup> this can be a result of EIE operating that favor productive intermediates in which D resides in a higher vibrational oscillator (i.e. C–D over M–D). The study of alkane C–H activation,<sup>3-5,7</sup> and evidence for key – but fleeting in solution –  $\sigma$ -alkane intermediates,<sup>8,9</sup> have relied heavily upon KIE or EIE effects.

We have previously reported on the use of *in crystallo*,<sup>10</sup> solid-state molecular organometallic (SMOM) chemistry to isolate and characterize cationic  $\sigma$ -alkane complexes of Rh and Co by single-crystal to single-crystal (SC-SC) solid/gas hydrogenation of an alkene precursor.<sup>11-13</sup> The secondary microenvironment provided by supporting  $[\text{BAR}^{\text{F}}_4]^-$  anions  $[\text{Ar}^{\text{F}} = 3,5-(\text{CF}_3)_2\text{C}_6\text{H}_3]$  is crucial in stabilizing weak 3-centre 2-electron  $\text{M}\cdots\text{H}-\text{C}$  bonding, meaning these complexes can be isolated and structurally characterized. However, for one precursor,  $[\text{Rh}(\text{Cy}_2\text{P}(\text{CH}_2)_3\text{PCy}_2)(\text{COD})][\text{BAR}^{\text{F}}_4]$ , **[1-COD][BAR<sup>F</sup><sub>4</sub>]** (COD = cyclooctadiene), the formed alkane, cyclooctane (COA), does not remain bound to the metal<sup>14</sup> when analyzed by X-ray crystallography after 3 hrs hydrogenation. Instead a Rh(I) cation with agostic<sup>15</sup> interactions from the cyclohexyl groups is

**Scheme 1. (A) Previously reported SC-SC hydrogenation of [1-COD][BAR<sup>F</sup><sub>4</sub>] to form [1][COA $\sigma$ BAR<sup>F</sup><sub>4</sub>]. [1]<sup>+</sup> = [Rh(L<sub>2</sub>)]<sup>+</sup>, L<sub>2</sub> = Cy<sub>2</sub>PCH<sub>2</sub>CH<sub>2</sub>CH<sub>2</sub>PCy<sub>2</sub>. (B) This work.**



formed, with the liberated COA encapsulated in an octahedral array of  $[\text{BAR}^{\text{F}}_4]^-$  anions: **[1][COA $\sigma$ BAR<sup>F</sup><sub>4</sub>]**, Scheme 1A. This multi-step reaction involves sequential alkene hydrogenation and loss of COA, presumably via an intermediate  $\sigma$ -cyclooctane complex. We now report that by following the progress of this solid/gas reaction with  $\text{H}_2$  or  $\text{D}_2$ , using a variety of methods, an

inverse isotope effect is revealed, leverage of which using D<sub>2</sub> allows for the optimal temporal window to be determined for structural characterization of the intermediate  $\sigma$ -cyclooctene complex. Extensive H/D exchange at the alkane has also occurred – exchange that is promoted by the solid-state microenvironment. These observations add to the isotope effects previously reported in solid-state organometallic reactivity,<sup>11,16–20</sup> which are still rare compared to those that occur in solution.<sup>1,5,7</sup>

## RESULTS AND DISCUSSION

**Reaction with H<sub>2</sub> and reassignment of the final product in the solid state.** As discussed, we have previously shown that addition of H<sub>2</sub> to single crystals of [1-COD][BARF<sub>4</sub>] for 3 hours results in hydrogenation of the COD in a solid/gas reaction. Analysis of selected crystals, albeit weakly diffracting, by X-ray diffraction (Diamond Light Source, Beamline I19) provided a structural solution of [1][COA $\bar{C}$ BARF<sub>4</sub>].<sup>14</sup> We now show that while this host/guest motif is indeed formed, it is in fact an intermediate and extended reaction times with H<sub>2</sub> result in an amorphous hydride-containing species as the final product. Nevertheless the overall reaction to form [1][COA $\bar{C}$ BARF<sub>4</sub>] is a SC-SC<sup>10</sup> transformation that hydrogenates COD to COA, presumably via a cyclooctene (COE) intermediate.

The reaction was initially followed in situ on bulk samples of finely crushed and sieved [1-COD][BARF<sub>4</sub>] (~50 mg, 71–150  $\mu$ m particle size) using solid-state <sup>31</sup>P{<sup>1</sup>H} NMR spectroscopy (SSNMR). Repeated exposure of an uncapped solid-state rotor to H<sub>2</sub> or D<sub>2</sub> (1.5 bar, 293 K), capping, and analysis provided a temporal evolution for H<sub>2</sub> and D<sub>2</sub> addition, Figure 1A. This reveals speciation in which [1-COD][BARF<sub>4</sub>] [ $\delta$  15.5,  $J(\text{RhP})$  ~120 Hz, apparent triplet due to crystallographically inequivalent P-environments]<sup>14</sup> is initially consumed to sequentially afford complexes assigned as [1-COE][BARF<sub>4</sub>], [1-COA][BARF<sub>4</sub>], [1][COA $\bar{C}$ BARF<sub>4</sub>] and finally hydride [Rh(Cy<sub>2</sub>P(CH<sub>2</sub>)<sub>3</sub>PCy<sub>2</sub>)H<sub>x</sub>][BARF<sub>4</sub>], [1-H<sub>x</sub>][BARF<sub>4</sub>]. The evolution of this system is first presented for H<sub>2</sub> addition, to baseline observations using D<sub>2</sub> that are discussed later.

After 20 minutes exposure of [1-COD][BARF<sub>4</sub>] to H<sub>2</sub> a new major species (~70%) is observed at  $\delta$  55.0 [apparent triplet  $J(\text{RhP})$  = 182 Hz]. The downfield shift and increased <sup>103</sup>Rh-<sup>31</sup>P coupling constant (due to a weak trans influence  $\sigma$ -alkane ligand) identify this as a  $\sigma$ -alkane complex, [Rh(Cy<sub>2</sub>P(CH<sub>2</sub>)<sub>3</sub>PCy<sub>2</sub>)(COA)][BARF<sub>4</sub>], [1-COA][BARF<sub>4</sub>], in

comparison with other – well defined – systems.<sup>14,21</sup> Also observed, in similar proportions to one another (~5–15%), are [1-COD][BARF<sub>4</sub>], and broad signals at  $\delta$  28.9 and  $\delta$  58.9. On the basis of their chemical shifts and temporal evolution these are assigned to [Rh(Cy<sub>2</sub>P(CH<sub>2</sub>)<sub>3</sub>PCy<sub>2</sub>)(COE)][BARF<sub>4</sub>], [1-COE][BARF<sub>4</sub>], and [1][COA $\bar{C}$ BARF<sub>4</sub>] respectively. [1-COE][BARF<sub>4</sub>] is proposed to have a structure as shown in Figure 1B (i.e. an alkene/agostic motif) on the basis of previously reported mono-alkene complexes formed in solid/gas reactions, such as [Rh(Cy<sub>2</sub>P(CH<sub>2</sub>)<sub>3</sub>PCy<sub>2</sub>)-(propene)][BARF<sub>4</sub>].<sup>22</sup> Such complexes can undergo rapid 1,3-hydrogen shifts (double bond isomerization) in the solid-state and it is likely that similar processes are operating for [1-COE][BARF<sub>4</sub>], *vide infra*. The encapsulated alkane complex [1][COA $\bar{C}$ BARF<sub>4</sub>] has a bis-agostic structure in which two C–H···Rh interactions come from the cyclohexyl groups rather than an alkane,<sup>14</sup> and thus would be expected to show very similar chemical shifts and coupling constants to [1-COA][BARF<sub>4</sub>] in the <sup>31</sup>P{<sup>1</sup>H} SSNMR spectrum. While  $J(\text{RhP})$  could not be resolved in this broad peak, the isotopologue formed using D<sub>2</sub> does show an apparent, broad, triplet structure for the  $\delta$  59.9 signal [ $J(\text{RhP})$  ~190 Hz], similar to [1-COA][BARF<sub>4</sub>] (Figure 1A, 40 mins D<sub>2</sub>).

After 40 minutes exposure to H<sub>2</sub> the complete consumption of [1-COD][BARF<sub>4</sub>] has occurred, [1-COE][BARF<sub>4</sub>] is still observed but at a lower relative proportion, and [1][COA $\bar{C}$ BARF<sub>4</sub>] has grown in. Initially surprising to us was that [1][COA $\bar{C}$ BARF<sub>4</sub>] is not the final product. Further exposure to H<sub>2</sub> resulted in the formation, after 3 hours, of a new complex, identified by two signals at  $\delta$  51 and  $\delta$  55 with coupling to <sup>103</sup>Rh not resolved, masked in the line width of the signals (fwhm = ~335 Hz). In our initial report of the characterization of [1][COA $\bar{C}$ BARF<sub>4</sub>] using SC-SC techniques, we correlated the structural solution (from weakly diffracting crystals selected from the reaction ensemble after 3 hrs reaction) with these two signals in the <sup>31</sup>P{<sup>1</sup>H} SSNMR spectrum.<sup>14</sup> We now suggest this assignment was wrong, and that these signals are in fact due to a complex that has undergone further addition of H<sub>2</sub> to form a Rh(III) complex of general formula [Rh(Cy<sub>2</sub>P(CH<sub>2</sub>)<sub>3</sub>PCy<sub>2</sub>)H<sub>x</sub>][BARF<sub>4</sub>], [1-H<sub>x</sub>][BARF<sub>4</sub>].

A number of observations support this new interpretation. (i) Dissolving this final product in d<sub>3</sub>-MeCN after removal of excess H<sub>2</sub> under vacuum forms the Rh(I) complex

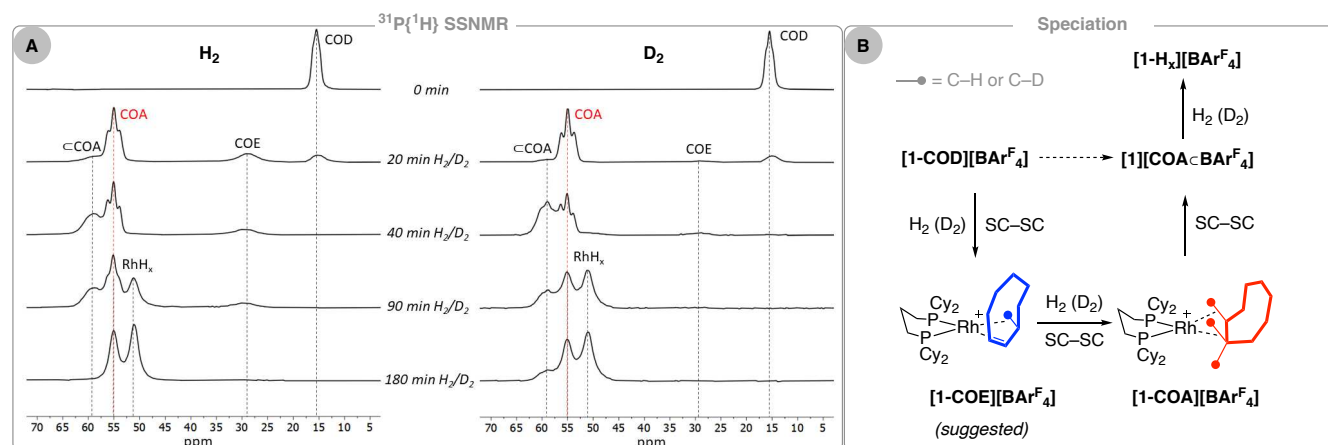
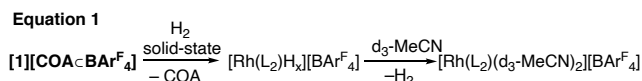


**Figure 1. A)** Evolution of the products from addition of H<sub>2</sub> or D<sub>2</sub> to crystalline [1-COD][BARF<sub>4</sub>] (1.5 bar, 293 K), measured by <sup>31</sup>P{<sup>1</sup>H} SSNMR spectroscopy (10 kHz spin rate, 273 K). Dotted lines to guide the eye. **B)** Solid-state speciation.

[Rh(Cy<sub>2</sub>P(CH<sub>2</sub>)<sub>3</sub>PCy<sub>2</sub>)(d<sub>3</sub>-MeCN)<sub>2</sub>][BAR<sup>F</sup><sub>4</sub>]<sup>23</sup> with the observation of dissolved H<sub>2</sub> [δ 4.57], from reductive elimination,<sup>24</sup> and free COA (Equation 1). (ii) The reduced magnitude of *J*(RhP) is indicative of a Rh(III) center. (iii) The formation of hydride species in related systems by solid/gas reactivity has been reported previously.<sup>19,25-27,29</sup> The rapid loss of H<sub>2</sub> means we cannot comment on the precise number of hydrogen ligands, i.e. Rh(H)<sub>2</sub> or Rh(H<sub>2</sub>)(H)<sub>2</sub>, or whether the Rh complex is still monomeric or has dimerized through bridging hydrides with a resulting loss of crystallinity.<sup>25,26</sup> However, what is now clear is that this final species is *not* [1][COA⊂BAR<sup>F</sup><sub>4</sub>] as initially proposed. This highlights the potential problems associated with the analysis of a solitary single-crystal by diffraction techniques and correlation with bulk analytical methods (e.g. NMR spectroscopy). As the final product [1-H<sub>x</sub>][BAR<sup>F</sup><sub>4</sub>] has lost long-range order (i.e. no discrete Bragg peaks) we suggest that even though it is the only species observed by <sup>31</sup>P{<sup>1</sup>H} SSNMR spectroscopy, manual crystal selection biases towards a very small proportion of [1][COA⊂BAR<sup>F</sup><sub>4</sub>] that is still present, and thus our previously reported structural characterization.<sup>14</sup>



As the reaction with H<sub>2</sub> up until [1][COA⊂BAR<sup>F</sup><sub>4</sub>] retains crystallinity, guided by the <sup>31</sup>P{<sup>1</sup>H} SSNMR data, we attempted to study the SC-SC reaction on suitably sized crystals (~0.2 × ~0.1 × ~0.05 mm), at time points between 20 and 90 minutes using single crystal X-ray diffraction. While structural solutions could be found for the [BAR<sup>F</sup><sub>4</sub>]<sup>−</sup> anions, the metal fragments were heavily disordered, likely superpositions of [1-COD][BAR<sup>F</sup><sub>4</sub>], [1-COE][BAR<sup>F</sup><sub>4</sub>], [1-COA][BAR<sup>F</sup><sub>4</sub>], and [1][COA⊂BAR<sup>F</sup><sub>4</sub>] in varying proportions.

**Reaction with D<sub>2</sub> and the crystallographic characterization of a σ-cycloalkane complex.** The solid/gas reaction of finely crushed and sieved [1-COD][BAR<sup>F</sup><sub>4</sub>] with D<sub>2</sub> was followed in situ using the same protocol as for H<sub>2</sub>. While this showed the equivalent set of sequential events occurring to ultimately form

[1-D<sub>x</sub>][BAR<sup>F</sup><sub>4</sub>], Figure 1, a *qualitative* comparison of the evolution of the system provides insight into any isotope effects that are operating. Firstly, [1-COD][BAR<sup>F</sup><sub>4</sub>] is completely consumed in the same timescale as for H<sub>2</sub> (40 mins), suggesting that no (or small at best) isotope effect is operating for the first hydrogenation of COD. Secondly, d<sub>x</sub>-[1-COE][BAR<sup>F</sup><sub>4</sub>] is processed faster with D<sub>2</sub>, so at the 40 mins time point the solid mixture analyses as essentially only d<sub>x</sub>-[1-COA][BAR<sup>F</sup><sub>4</sub>] and d<sub>x</sub>-[1][COA⊂BAR<sup>F</sup><sub>4</sub>]. This suggests an inverse isotope effect is operating for the formation of d<sub>x</sub>-[1-COA][BAR<sup>F</sup><sub>4</sub>] from [1-COE][BAR<sup>F</sup><sub>4</sub>]. Finally the system evolves to give the final product, [1-D<sub>x</sub>][BAR<sup>F</sup><sub>4</sub>], but its formation is slower with D<sub>2</sub>, as after 3 hrs some d<sub>x</sub>-[1][COA⊂BAR<sup>F</sup><sub>4</sub>] remains. This suggests a normal isotope effect is operating for the formation of this hydride species. These isotope effects will be discussed in more detail later.

This reaction was repeated with D<sub>2</sub> on larger single crystalline material. By optimizing the time of D<sub>2</sub> addition a structural solution for d<sub>x</sub>-[1-COA][BAR<sup>F</sup><sub>4</sub>] could be obtained after 40 minutes using single-crystal X-ray diffraction.<sup>28</sup> While the data analysis was complicated by pseudo-merohedral twinning and superpositionality disordered minor components of [1-COD][BAR<sup>F</sup><sub>4</sub>] and d<sub>x</sub>-[1-COE][BAR<sup>F</sup><sub>4</sub>] the structural solution is unambiguous (*R* = 7.15%) and reveals a [Rh(Cy<sub>2</sub>PCH<sub>2</sub>CH<sub>2</sub>CH<sub>2</sub>PCy<sub>2</sub>)]<sup>+</sup> fragment bound with a cyclooctane ligand, Figure 2A. This successful structural solution relied upon the combination of isotope effects operating, as discussed above, that favored d<sub>x</sub>-[1-COA][BAR<sup>F</sup><sub>4</sub>] being formed in compositionally purer form compared with H<sub>2</sub> addition. Full details of the refinement can be found in the Supporting Materials.

The cation in d<sub>x</sub>-[1-COA][BAR<sup>F</sup><sub>4</sub>] has a pseudo square planar Rh(I) center, which is coordinated on one side by the chelating phosphine [Rh-P = 2.221(3), 2.196(2) Å] and the other by the cyclooctane ligand. C-C bond distances in the COA ligand were unrestrained and fall in the range 1.44(2)–1.60(2) Å, consistent with single bonds and confirming full hydrogenation of

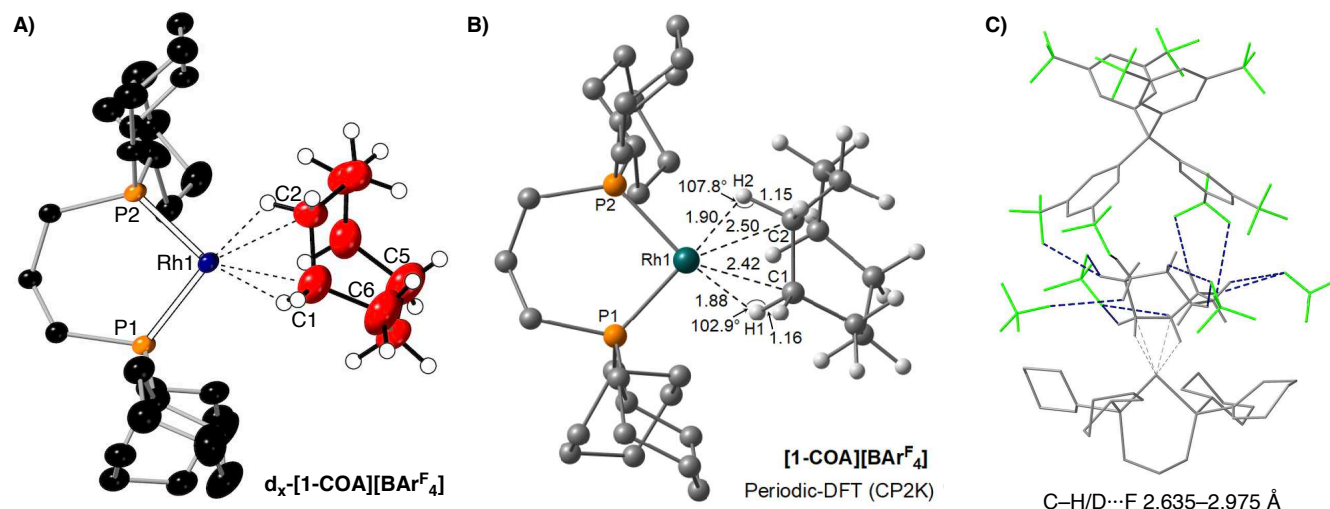


**Figure 2.** (A) Single-crystal X-ray structure of the cation in d<sub>x</sub>-[1-COA][BAR<sup>F</sup><sub>4</sub>] (110 K, 30% displacement ellipsoids, selected calculated H/D-atoms shown). Selected bond lengths (Å) and angles (°) [1-COA][BAR<sup>F</sup><sub>4</sub>]: Rh-P1, 2.221(3); Rh-P2, 2.196(2); Rh-C1, 2.40(1); Rh-C2, 2.48(1); C1-C2, 1.49(2); C5-C6, 1.60(2) P1RhP2/RhC1C2 = 2.6(9). (B) Periodic DFT calculated structure of [1-COA][BAR<sup>F</sup><sub>4</sub>]. (C) Orientation of the cation and CF<sub>3</sub> groups from proximal anions highlighting the C-H/D...F non-covalent interactions.

the COD. The COA ligand engages in a 1,2-motif  $\sigma$ -bond interaction with rhodium, as signaled by the Rh...C distances from adjacent C-atoms [C1, C2; 2.40(1), 2.48(1) Å], being similar to those found for other alkane ligands that bind in a 1,2-motif with this, or related, Rh-fragments, e.g. norbornane [2.408(2), 2.402(2) Å],<sup>14</sup> isobutane [2.36(2), 2.442(7) Å]<sup>11</sup> and 2-methylbutane [2.348(9), 2.39(1) Å].<sup>13</sup> Hydrogen (deuterium) atoms were not located. Periodic DFT calculations (Figure 2B) reproduce the structure well, capturing the slight asymmetry in the Rh...C distances [calc. 2.43 and 2.50 Å], and highlight the elongation of the C–H bonds engaged in the C–H  $\rightarrow$  Rh  $\sigma$ -interactions (ca. 1.15 Å). They also show that the COA ligand binds in an  $\eta^2, \eta^2$  motif, [Rh(Cy<sub>2</sub>PCH<sub>2</sub>CH<sub>2</sub>CH<sub>2</sub>PCy<sub>2</sub>)( $\eta^2, \eta^2$ -COA)][BAR<sup>F</sup><sub>4</sub>], as found for the norbornane analogue.<sup>14</sup> The Rh...C distances are shorter than found in the Rh(III) complex [RhH( $\kappa^3$ -Cy<sub>2</sub>P(CH<sub>2</sub>)<sub>2</sub>CH(CH<sub>2</sub>)<sub>2</sub>PCy<sub>2</sub>)(COA)][BAR<sup>F</sup><sub>4</sub>], 2.90(3) Å, where a  $\eta^1$ -coordination mode is observed for COA. The alkane ligand in d<sub>x</sub>-[1-COA][BAR<sup>F</sup><sub>4</sub>] sits in a pocket defined by the proximal [BAR<sup>F</sup><sub>4</sub>]<sup>−</sup> anions, Figure 2C, and there are a number of relatively close C–H...F contacts that act to further stabilize the complex – as described before for other alkane complexes of this type.<sup>13,29,30</sup> QTAIM, non-covalent interaction plots and NBO analyses support the assigned hapticity and micro-environment effects (Supporting Materials).

Cyclooctane complexes have been identified as early intermediates in C–H activation, using fast time resolved infrared techniques, having lifetimes on the ns- $\mu$ s timescale e.g. Rh( $\eta^5$ -C<sub>5</sub>Me<sub>5</sub>)(CO)(cyclooctane)<sup>31</sup> and Tp\*Rh(CNR)-(cyclooctane).<sup>32</sup>  $\sigma$ -Alkane complexes of cyclooctane have also been identified as intermediates in alkane dehydrogenation reactions using computational methods.<sup>33</sup> The isolation of [1-COA][BAR<sup>F</sup><sub>4</sub>] thus represents a structurally authenticated example that has a significant lifetime at 293 K. Attempts to characterize [1-COA][BAR<sup>F</sup><sub>4</sub>] or [1-COE][BAR<sup>F</sup><sub>4</sub>] by low temperature solution NMR spectroscopy<sup>8,34,35</sup> (CD<sub>2</sub>Cl<sub>2</sub>, 183 K) led to the formation of intractable solids.

Exposure of single crystals of [1-COD][BAR<sup>F</sup><sub>4</sub>] to D<sub>2</sub> for a total of 60 minutes and analysis of selected crystals by single crystal X-ray diffraction resulted in a structural refinement that confirmed the formation of d<sub>x</sub>-[1][COA][BAR<sup>F</sup><sub>4</sub>] (Supporting Materials), but due to a drop off in data quality, alongside significant superpositional disorder, this only provided atom connectivity. Nevertheless this confirms the previous report of the formation of this complex in a SC-SC reaction.<sup>14</sup>

**Quantification of the isotope effects of the solid/gas reaction using JMAK analysis.** The time course of these solid/gas reactions was followed using solution quenching experiments, that determine the relative ratios of COD, COE and COA. Starting from [1-COD][BAR<sup>F</sup><sub>4</sub>] the same method described for the <sup>31</sup>P{<sup>1</sup>H} SSNMR experiments was used for individual samples that were exposed, over incrementally longer reactions times, to either H<sub>2</sub> or D<sub>2</sub> in NMR tubes (Figure 3A, 7.6 mg each sample, 1.5 bar, 293 K). Each of these was quenched by evacuation, refilling with Ar, and addition of a suitable coordinating solvent. Using d<sub>6</sub>-acetone a mixture of [Rh(Cy<sub>2</sub>P(CH<sub>2</sub>)<sub>3</sub>PCy<sub>2</sub>)(d<sub>6</sub>-acetone)<sub>2</sub>][BAR<sup>F</sup><sub>4</sub>],<sup>23</sup> displaced COE and COA, and unreacted [1-COD][BAR<sup>F</sup><sub>4</sub>] are formed. Analysis by solution <sup>31</sup>P{<sup>1</sup>H} and <sup>1</sup>H NMR spectroscopy allowed the ratios of COD, COE and COA to be determined by integration relative to [BAR<sup>F</sup><sub>4</sub>]<sup>−</sup>. Further addition of d<sub>3</sub>-MeCN to these solutions liberated bound COD, forming [Rh(Cy<sub>2</sub>P(CH<sub>2</sub>)<sub>3</sub>PCy<sub>2</sub>)(d<sub>3</sub>-MeCN)<sub>2</sub>][BAR<sup>F</sup><sub>4</sub>],<sup>23</sup> and the resulting COA/COE/COD ensemble was analyzed

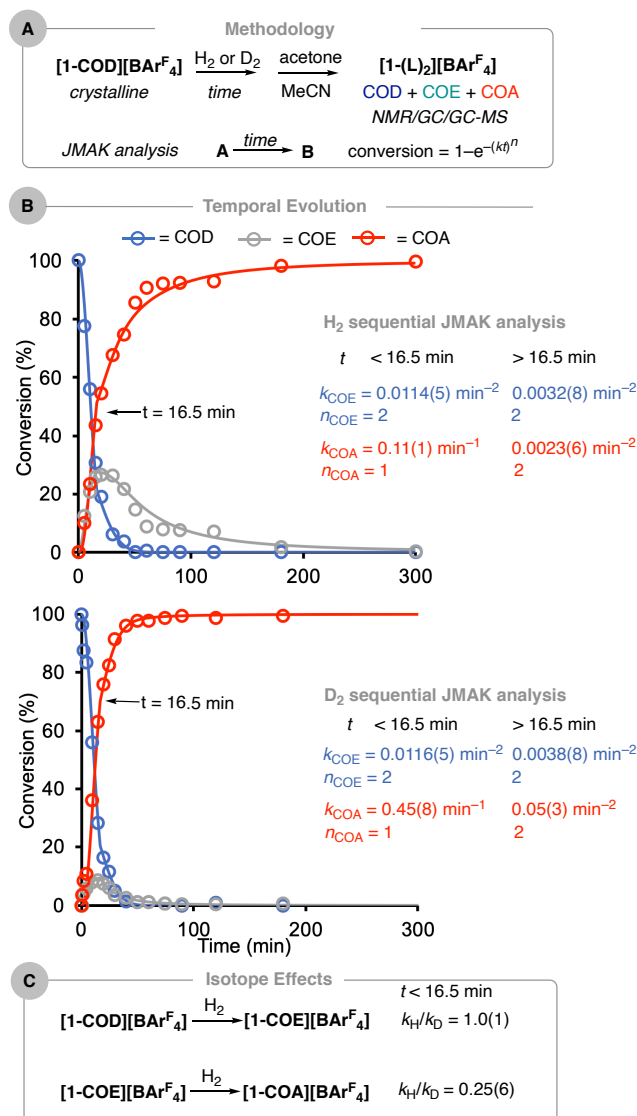


**Figure 3.** (A) Methodology for temporal analysis (L<sub>2</sub> = d<sub>3</sub>-MeCN or d<sub>6</sub>-acetone) and simple JMAK analysis. (B) Temporal evolution: each data point a separate experiment (1.5 bar H<sub>2</sub> or D<sub>2</sub>, 293 K); sequential JMAK analysis fits with growth rate ( $k$ ) and Avrami ( $n$ ) constants:  $k/n_{\text{COE}}$  refers to [COD]<sub>total</sub> to [COE]<sub>total</sub>;  $k/n_{\text{COA}}$  refers to [COE]<sub>total</sub> to [COA]<sub>total</sub> and do not reflect actual speciation. (C) Calculated isotope effects for the SC-SC organometallic transformation before  $t = 16.5$  mins.

using GC-MS for H<sub>2</sub> and D<sub>2</sub> additions. Both methods give very similar temporal profiles for H<sub>2</sub> addition, but GC-MS-derived data allow for quantification of both H<sub>2</sub> and D<sub>2</sub> addition without interference from additional H/D exchange processes (*vide infra*) that affects analysis by <sup>1</sup>H NMR spectroscopy.<sup>36</sup> These data were then used as a proxy for the organometallic solid-state reactivity that is occurring. As this methodology determines [COA]<sub>TOTAL</sub>, and does not discriminate between bound or free alkane, it reports on the ensemble of [1-COA][BAR<sup>F</sup><sub>4</sub>], [1][COA][BAR<sup>F</sup><sub>4</sub>] and [1-H<sub>x</sub>][BAR<sup>F</sup><sub>4</sub>]. However, the rate of change of [COA]<sub>TOTAL</sub> formation describes [1-COA][BAR<sup>F</sup><sub>4</sub>], as this is the first formed species in this set.

Figure 3B presents the resulting reaction course plots for H<sub>2</sub> and D<sub>2</sub> addition, over a 5 hour sampling period. Qualitatively, both show the same rate of consumption of [1-COD][BAR<sup>F</sup><sub>4</sub>], that is

complete after 40 minutes. COE is observed to be formed as an intermediate, but its relative maximum is lower, and COA is formed faster, for D<sub>2</sub> addition. This signals faster progress of COE to COA using D<sub>2</sub>, i.e. an inverse isotope effect as suggested from the complementary <sup>31</sup>P{<sup>1</sup>H} SSNMR experiments described earlier.

The same batch of sieved crystalline material was used for each of the individual H<sub>2</sub> and D<sub>2</sub> experiments shown in Fig. 3B. Repeating selected data points using a different batch of crystalline materials (Supporting Materials) showed a small amount of variability between batches, but the data are still fully consistent with the overall temporal profiles recorded for the main experiments. This may be due to surface area effects for different crystalline batches or other experimental variables (e.g. small changes in the pressure of H<sub>2</sub> or D<sub>2</sub>).

These data have been analyzed using a sequential Johnson–Mehl–Avrami–Kolmogorov (JMAK)<sup>37,38</sup> solid-state kinetic model for an A → B → C reaction sequence (see Supporting Materials for full derivation and implementation). Figure 3B shows the resulting fits (solid-lines). JMAK analysis describes the progress of a solid-state reaction, i.e. A → B, by a nucleation and growth model, where *k* is the growth rate constant and *n* is the Avrami exponent, Equation 2. Exponents close to *n* = 2, 3 and 4 have been suggested to be due to 1-D, 2-D and 3-D reaction growth dimensionality, respectively; while *n* = 1 suggests a non-cooperative process and can be related to classical first order processes in homogeneous systems.<sup>39</sup> JMAK analysis has been used to model simple SC-SC, A → B, processes.

11,13,40–42

$$\text{conversion} = 1 - e^{-(kt)^n} \quad (\text{Equation 2})$$

At the early stages of the reaction (<16.5 minutes) the values of *k* and *n* are the same within error for both H<sub>2</sub> and D<sub>2</sub> addition to [1-COD][BAR<sup>F</sup><sub>4</sub>] (*k* = 0.0114(5) min<sup>-2</sup> and 0.0116(5) min<sup>-2</sup> respectively; *n* = 2). Thus, there is no isotope effect observed for the hydrogenation of [1-COD][BAR<sup>F</sup><sub>4</sub>] to give [1-COE][BAR<sup>F</sup><sub>4</sub>], i.e. *k*(H)/*k*(D) = 1, Figure 3C. As the second addition of D<sub>2</sub> to [1-COE][BAR<sup>F</sup><sub>4</sub>] is faster than with H<sub>2</sub> (vide infra, Supporting Materials), and formation of [1-H<sub>x</sub>][BAR<sup>F</sup><sub>4</sub>] qualitatively shows a normal isotope effect, we suggest that hydrogenation is not diffusion limited. Rate-limiting substrate diffusion has been demonstrated for *in crystallo* organometallic reactivity in MOFs;<sup>17</sup> while inverse isotope effects have been noted for diffusion of H<sub>2</sub> or D<sub>2</sub> into microporous materials.<sup>43</sup> The structurally very close complex [Rh(Cy<sub>2</sub>P(CH<sub>2</sub>)<sub>3</sub>PCy<sub>2</sub>)(NBD)][BAR<sup>F</sup><sub>4</sub>] (NBD = norbornadiene) undergoes rapid SC-SC hydrogenation to form the corresponding σ-alkane complex in <5 mins (cf. [1-COD][BAR<sup>F</sup><sub>4</sub>] 40 minutes),<sup>14</sup> which also argues against rate limiting diffusion of H<sub>2</sub>. Instead, we propose a rate-limiting, possibly correlated, intramolecular dissociation of one of the alkene groups in COD. Pertinently, in solution, [Rh(chelating phosphine)(COD)]<sup>+</sup> complexes also undergo hydrogenation a lot slower than their NBD analogues, although the reasons behind this are not clear.<sup>44</sup>

This model is complicated by a subtle point of discontinuity at *t* = 16.5 mins for both H<sub>2</sub> and D<sub>2</sub> addition, which when included provides a better fit to the data. This reports back a reduced value for *k* for both H<sub>2</sub> (0.0032(8) min<sup>-2</sup>) and D<sub>2</sub> (0.0038(8) min<sup>-2</sup>) addition to [1-COD][BAR<sup>F</sup><sub>4</sub>] after 16.5 mins that are the same

within error, no change in *n*, and thus no measurable isotope effect. As this change occurs at the same point in time for both H<sub>2</sub> and D<sub>2</sub> addition we suggest this is not an experimental artifact, and is triggered at a certain conversion of [1-COD][BAR<sup>F</sup><sub>4</sub>]. As microcracking of single crystals,<sup>45</sup> would be expected to increase the rate of conversion through surface area arguments, we speculate that this change is to do with a correlated,<sup>46</sup> but subtle, change in the spatially averaged periodic structure, that occurs in hydrogenation of [1-COD][BAR<sup>F</sup><sub>4</sub>]. Repeating these experiments on larger single crystals and measurement of the unit cell parameters with time showed no significant step change in axes lengths that would signal a phase change.

In contrast to the consumption of [1-COD][BAR<sup>F</sup><sub>4</sub>], the subsequent hydrogenation of [1-COE][BAR<sup>F</sup><sub>4</sub>] is significantly faster for D<sub>2</sub> addition than H<sub>2</sub> (*k* = 0.45(8) min<sup>-1</sup> vs 0.11(1) min<sup>-1</sup> respectively) at the initial stages of the reaction, and the Avrami exponent is now unity for both. There is thus an inverse isotope effect observed: *k*(H)/*k*(D) = 0.25(5). Post 16.5 minutes, *k* again decreases significantly, but *n* is now 2, and there is also a significant inverse isotope effect, *k*(H)/*k*(D) = 0.05(3) (*k* = 0.0023(6) min<sup>-2</sup> vs 0.04(2) min<sup>-2</sup>). The change in “dimensionality”, *n*, makes direct comparison difficult between the two regimes. Interestingly, in line with Finke’s suggestion that *k* and *n* are convoluted and cannot be easily separated,<sup>38</sup> for this *n* = 2 regime  $\sqrt{k(H)}/\sqrt{k(D)} = 0.25(6)$ , which is the same as for the pre-16.5 mins value (*n* = 1). The consequence of these combined inverse isotope effects for [1-COE][BAR<sup>F</sup><sub>4</sub>] hydrogenation is that after 40 minutes the conversion of COD to COA is essentially complete using D<sub>2</sub>, but considerable (~20%) COE still remains when using H<sub>2</sub>.

**H/D exchange in COE and COA and the inverse isotope effect.** The evolution of the reaction between [1-COD][BAR<sup>F</sup><sub>4</sub>] and D<sub>2</sub> was monitored using GC-MS on the same finely powdered samples as used for the quenching experiments. This showed that significant, almost complete, H/D exchange was occurring into both COE and COA in this SC-SC solid/gas reaction. No H/D exchange was observed into COD. Figure 4 shows the resulting time course versus %D incorporation for COE and COA<sub>TOTAL</sub> using D<sub>2</sub>. After 40 minutes the remaining COE reaches ~95% D incorporation, with a weighted average ~d<sub>13</sub>-COE. High levels of exchange (~75% D, ~d<sub>11</sub>-COE) are achieved at the first measured time point of 2.5 mins. H/D exchange into [1-COE][BAR<sup>F</sup><sub>4</sub>] thus occurs rapidly. The temporal profile for H/D exchange in COA follows closely with that of COE, and not [COA]<sub>TOTAL</sub>, resulting in 68% D (~d<sub>11</sub>-COA) after 2.5 minutes, rising to 93% D incorporation after 40 mins. This suggests a formulation of ~d<sub>15</sub>-[1-COA][BAR<sup>F</sup><sub>4</sub>] for the crystallographically characterized sample (Figure 2A).

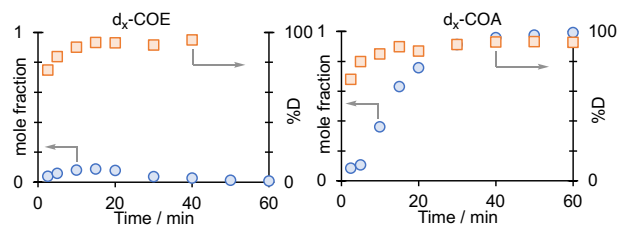
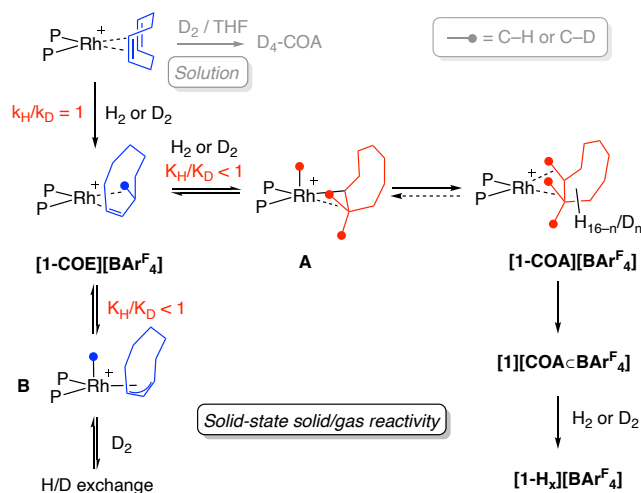


**Figure 4.** % H/D incorporation into COE/COA from addition of D<sub>2</sub> (1.5 bar) to crystalline [1-COD][BAR<sup>F</sup><sub>4</sub>], measured by GC/MS. ○ = mole fraction of COE/COA<sub>TOTAL</sub>. □ = %D incorporation relative to maximum possible. COE D incorporation data not available after

50 minutes due to weak signal to noise at very low COE mole fractions.

A plausible mechanism for this SC-SC H/D exchange process is shown in Scheme 2, that may also explain the inverse isotope effect observed for formation of  $[1\text{-COA}][\text{BAR}^{\text{F}_4}]$ .

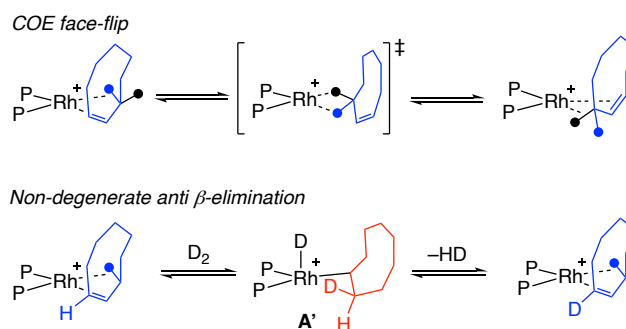
**Scheme 2. Suggested mechanism for H/D exchange in the solid-state.  $[\text{BAR}^{\text{F}_4}]$  anions are not shown.**



The initial, irreversible, addition of  $\text{H}_2/\text{D}_2$  to  $[1\text{-COD}][\text{BAR}^{\text{F}_4}]$  results in  $[1\text{-COE}][\text{BAR}^{\text{F}_4}]$ , for which no isotope effect is measured. Subsequent addition of  $\text{H}_2/\text{D}_2$  would form an alkyl hydride, **A**, followed by reductive bond formation to give  $[1\text{-COA}][\text{BAR}^{\text{F}_4}]$ . This would form  $\text{d}_4\text{-}[1\text{-COA}][\text{BAR}^{\text{F}_4}]$  with  $\text{D}_2$  – contrary to the higher levels of deuteration observed. That the levels of H/D incorporation in COA closely matches those for COE, even at low conversions to  $\text{COA}_{\text{TOTAL}}$ , suggests exchange occurs principally from  $[1\text{-COE}][\text{BAR}^{\text{F}_4}]$  and not  $[1\text{-COA}][\text{BAR}^{\text{F}_4}]$ . However, as H/D exchange has been reported for other well defined  $\sigma$ -alkane complexes we cannot rule out that this does not also occur here.<sup>11,18</sup> H/D exchange at  $[1\text{-COE}][\text{BAR}^{\text{F}_4}]$  could proceed by two routes: (a) formation of an alkyl deuteride, **A**, with  $\text{D}_2$  which if followed by  $\beta$ -elimination from a different  $\alpha$ -methylene group would return D-labelled  $[1\text{-COE}][\text{BAR}^{\text{F}_4}]$ ; (b) C–H activation of COE to form an alkyl hydride, **B**, H/D exchange with  $\text{D}_2$ , and a 1,3-deutride shift. Similar intermediates to **B** have been described for the solid-state hydrogenation of  $[\text{Ir}(\text{PPh}_3)_2(\text{COD})]_3[\text{PW}_{12}\text{O}_{40}]$ .<sup>19</sup> Both processes would result in double bond isomerization. Repetition exchanges all the C–H bonds for C–D, if combined with a process that allows for all C–H bonds to interact with the Rh-center (see below). Consistent with H/D exchange at a Rh–H intermediate that introduces a single D-atom, there is no enhancement of odd-or even numbers of  $\text{d}_x$  (Supporting Materials). These reversible processes must be thermodynamically balanced, and be connected by low barriers, for such rapid H/D exchange to occur. Periodic DFT calculations on hydride insertion/ $\beta$ -elimination show this to be the case for closely related  $[\text{Rh}(\text{Cy}_2\text{PCH}_2\text{CH}_2\text{PCy}_2)(\text{cyclohexene})][\text{BAR}^{\text{F}_4}]$  in the solid-state, with barriers being less than  $13.9 \text{ kcal mol}^{-1}$ .<sup>11</sup> A low barrier to a 1,3-hydride shift in the isomerization of propene in  $[\text{Rh}(\text{Cy}_2\text{PCH}_2\text{CH}_2\text{PCy}_2)(\text{propene})][\text{BAR}^{\text{F}_4}]$  has also been reported ( $10.9 \text{ kcal mol}^{-1}$ ) that operates via an allyl hydride intermediate.<sup>22</sup> H/D exchange at Rh(III)-H with  $\text{D}_2$  would likely operate via a  $\sigma$ -CAM mechanism.<sup>47,48</sup>

In order to achieve such high levels of deuteration in both COE and COA all the C–H bonds in the cyclic hydrocarbon need to interact with the metal center, and the pathways shown in Scheme 2 would result in only one face of COA being deuterated. Scheme 3 suggests routes that allow for both faces to be deuterated: a face flip of COE; or a non-degenerate  $\beta$ -elimination of an anti-orientated C–H bond from intermediate **A'**, that may be promoted by ring strain in the cyclooctyl ligand.<sup>49</sup> Similarly high levels of H/D exchange in the resulting COA have also been reported in solid/gas reactions of  $[\text{Ir}(\text{PPh}_3)_2(\text{COD})]_3[\text{PW}_{12}\text{O}_{40}]$  with  $\text{D}_2$ .<sup>19</sup>

**Scheme 3. Suggested pathways that allow for per-deuteration**



Hydrogenation in THF solution of  $[1\text{-COD}][\text{BAR}^{\text{F}_4}]$  results in the formation of  $\text{d}_4\text{-COA}$  with no H/D exchange observed. Thus the, solvent-free, microenvironment provided by the  $[\text{BAR}^{\text{F}_4}]^-$  anions, that prevents rapid loss of the bound COE (and COA), facilitates the extremely high levels of H/D exchange in this SC-SC process.

The rapid deuteration of  $[1\text{-COE}][\text{BAR}^{\text{F}_4}]$  results in nearly complete H/D exchange of COE. This could lead to an inverse equilibrium isotope effect (EIE) being observed for the consumption of  $[1\text{-COE}][\text{BAR}^{\text{F}_4}]$ , as deuteration would be expected to bias any equilibria towards  $\text{d}_x\text{-}[1\text{-COE}][\text{BAR}^{\text{F}_4}]$ , and intermediate **A** (assuming a small, or even inverse,<sup>5</sup> isotope effect for  $\text{H}_2$  addition to  $[1\text{-COE}][\text{BAR}^{\text{F}_4}]$ ) and away from **B**. While this assumes reductive bond cleavage from **A** to form  $[1\text{-COA}][\text{BAR}^{\text{F}_4}]$  is rate determining, COA loss from  $[1\text{-COA}][\text{BAR}^{\text{F}_4}]$  to form  $[1][\text{COA}][\text{BAR}^{\text{F}_4}]$  could also be rate determining, as the solution quenching experiments do not discriminate between these two species in measuring  $[\text{COA}]_{\text{TOTAL}}$  (Figure 4).

This analysis is further complicated by a number of factors that are unique to the solid-state reactivity described here. The cumulative effects of thermodynamically favorable per-deuteration,<sup>50</sup> feasible because of the encapsulation, will induce a net secondary isotope effect on the reductive bond formation from **A**. Isotopologue induced changes in non-covalent interactions between the alkane and anion-microenvironment will also affect both the equilibrium thermodynamics and transition state energetics, and thus may also contribute to the observed isotope effects. Related binding isotope effects (BIE) have been observed with enzymes and molecular capsules on binding different isotopologues of the same guest substrate.<sup>2</sup> So while the observation of an inverse isotope effect in a SC-SC molecular organometallic solid/gas reaction is clear cut here, the additional complexity introduced by reactivity in the single-crystal makes the detailed analysis of the underlying reasons for this more challenging.

An inverse isotope effect has been reported for the solution-based deuteration of NBD using  $[\text{Ir}(\text{PPh}_3)_2\text{H}_2(\text{acetone})_2][\text{PF}_6]$ , and is explained by a mechanism that favors norbornyl-hydride intermediates, closely related to intermediates described here such as **A**.<sup>51</sup> Inverse EIE have previously been used to identify the intermediacy of  $\sigma$ -alkane complexes in overall reductive elimination of alkanes from alkyl-hydrides in solution where loss of the alkane from the metal center is rate determining.<sup>4</sup>

## CONCLUSIONS

The study of isotope effect has been central to the understanding of mechanism in organometallic synthesis and catalysis in the solution phase. The inverse isotope effect described here for the sequential SC-SC hydrogenation of **[1-COD][BAr<sup>F</sup><sub>4</sub>]** adds to the small number of reports where (albeit normal) isotope effects have been noted in molecular organometallic chemistry in the crystalline phase.<sup>11,16-20</sup> Leverage of the isotopologue-induced changes in relative rates results in the structural characterization of a  $\sigma$ -alkane complex of cyclooctane. While reactivity in the single-crystalline environment presents challenges in both data collection and analysis of isotope effects, the installed secondary microenvironment around the reactive metal center promotes temporal control over composition, stability ( $\sigma$ -alkane complex formation) and reactivity (extensive H/D exchange). This highlights that the advantages of isotopic substitution in the study of mechanism and synthesis are not unique to homogeneous systems and should also be considered as a useful tool in SC-SC transformations of molecular organometallics.

## ASSOCIATED CONTENT

### Supporting Information

Full details of synthesis, characterization (including single crystal X-ray determinations), kinetic measurement protocols, sequential JMAK analysis, CIF for **[1-COA][BAr<sup>F</sup><sub>4</sub>]**, connectivity-only structure for the redetermination of **[1][COA $\kappa$ -BAr<sup>F</sup><sub>4</sub>]** using D<sub>2</sub>; computational details and optimized structure of **[1-COA][BAr<sup>F</sup><sub>4</sub>]** (.xyz file).

## AUTHOR INFORMATION

### Corresponding Authors

\* [laurence.doyle@york.ac.uk](mailto:laurence.doyle@york.ac.uk), [S.A.Macgregor@hw.ac.uk](mailto:S.A.Macgregor@hw.ac.uk), [andrew.weller@york.ac.uk](mailto:andrew.weller@york.ac.uk)

### Notes

† Present address: Centro de Investigación en Química Sostenible (CIQSO), Edificio Robert H Grubbs, Campus de El Carmen, Universidad de Huelva 21007 Huelva (Spain)

The authors declare no competing financial interests

## ACKNOWLEDGMENT

EPSRC (EP/M024210/2) and SCG chemicals for funding.

## REFERENCES

- (1) Simmons, E. M.; Hartwig, J. F. On the Interpretation of Deuterium Kinetic Isotope Effects in CH Bond Functionalizations by Transition-Metal Complexes, *Angew. Chem. Int. Ed.* **2012**, *51*, 3066-3072.
- (2) Świderek, K.; Paneth, P. Binding Isotope Effects, *Chem. Rev.* **2013**, *113*, 7851-7879.

- (3) Sattler, A. Hydrogen/Deuterium (H/D) Exchange Catalysis in Alkanes, *ACS Catal.* **2018**, *8*, 2296-2312.
- (4) Jones, W. D. Isotope Effects in C–H Bond Activation Reactions by Transition Metals, *Acc. Chem. Res.* **2003**, *36*, 140-146.
- (5) Bullock, R. M.; Bender, B. R. In *Encyclopedia of Catalysis*; John Wiley & Sons, 2002.
- (6) Parkin, G. Temperature-Dependent Transitions between Normal and Inverse Isotope Effects Pertaining to the Interaction of H–H and C–H Bonds with Transition Metal Centers, *Acc. Chem. Res.* **2009**, *42*, 315-325.
- (7) Truong, P. T.; Miller, S. G.; McLaughlin Sta. Maria, E. J.; Bowring, M. A. Large Isotope Effects in Organometallic Chemistry, *Chem. Eur. J.* **2021**, *27*, 14800-14815.
- (8) Hall, C.; Perutz, R. N. Transition Metal Alkane Complexes, *Chem. Rev.* **1996**, *96*, 3125-3146.
- (9) Weller, A. S.; Chadwick, F. M.; McKay, A. I. Transition Metal Alkane-Sigma Complexes *Adv. Organomet. Chem.*, **2016**; *66*, 223-276
- (10) Reid, K. A.; Powers, D. C. In *Crystalline Organometallic Chemistry*, *Chem. Commun.* **2021**, *57*, 4993-5003.
- (11) McKay, A. I.; Bukvic, A. J.; Tegner, B. E.; Burnage, A. L.; Martínez-Martínez, A. J.; Rees, N. H.; Macgregor, S. A.; Weller, A. S. Room Temperature Acceptorless Alkane Dehydrogenation from Molecular  $\sigma$ -Alkane Complexes, *J. Am. Chem. Soc.* **2019**, *141*, 11700-11712.
- (12) Boyd, T. M.; Tegner, B. E.; Tizzard, G. J.; Martínez-Martínez, A. J.; Neale, S. E.; Hayward, M. A.; Coles, S. J.; Macgregor, S. A.; Weller, A. S. A Structurally Characterized Cobalt(I)  $\sigma$ -Alkane Complex, *Angew. Chem. Int. Ed.* **2020**, *59*, 6177-6181.
- (13) Bukvic, A. J.; Burnage, A. L.; Tizzard, G. J.; Martínez-Martínez, A. J.; McKay, A. I.; Rees, N. H.; Tegner, B. E.; Krämer, T.; Fish, H.; Warren, M. R.; Coles, S. J.; Macgregor, S. A.; Weller, A. S. A Series of Crystallographically Characterized Linear and Branched  $\sigma$ -Alkane Complexes of Rhodium: From Propane to 3-Methylpentane, *J. Am. Chem. Soc.* **2021**, *143*, 5106-5120.
- (14) Martínez-Martínez, A. J.; Tegner, B. E.; McKay, A. I.; Bukvic, A. J.; Rees, N. H.; Tizzard, G. J.; Coles, S. J.; Warren, M. R.; Macgregor, S. A.; Weller, A. S. Modulation of  $\sigma$ -Alkane Interactions in  $[\text{Rh}(\text{L}_2)(\text{alkane})]^+$  Solid-State Molecular Organometallic (SMOM) Systems by Variation of the Chelating Phosphine and Alkane: Access to  $\eta^2$ ,  $\eta^2$ - $\sigma$ -Alkane Rh(I),  $\eta^1$ - $\sigma$ -Alkane Rh(III) Complexes, and Alkane Encapsulation, *J. Am. Chem. Soc.* **2018**, *140*, 14958-14970.
- (15) Brookhart, M.; Green, M. L. H.; Parkin, G. Agostic Interactions in Transition Metal Compounds, *Proc. Nat. Acad. Sci. (USA)* **2007**, *104*, 6908.
- (16) Wang, C.-H.; Gao, W.-Y.; Powers, D. C. Measuring and Modulating Substrate Confinement During Nitrogen-Atom Transfer in a Ru<sub>2</sub>-Based Metal-Organic Framework, *J. Am. Chem. Soc.* **2019**, *141*, 19203-19207.
- (17) Wang, C.-H.; Das, A.; Gao, W.-Y.; Powers, D. C. Probing Substrate Diffusion in Interstitial MOF Chemistry with Kinetic Isotope Effects, *Angew. Chem. Int. Ed.* **2018**, *57*, 3676-3681.
- (18) Chadwick, F. M.; Krämer, T.; Gutmann, T.; Rees, N. H.; Thompson, A. L.; Edwards, A. J.; Buntkowsky, G.; Macgregor, S. A.; Weller, A. S. Selective C–H Activation at a Molecular Rhodium Sigma-Alkane Complex by Solid/Gas Single-Crystal to Single-Crystal H/D Exchange, *J. Am. Chem. Soc.* **2016**, *138*, 13369-13378.
- (19) Siedle, A. R.; Newmark, R. A.; Sahyun, M. R. V.; Lyon, P. A.; Hunt, S. L.; Skarjune, R. P. Solid-State Chemistry of Molecular Metal Oxide Clusters. Multiple, Sequential Carbon-Hydrogen Activation Processes in the Hydrogenation of Coordinated Cyclooctene. Lattice Mobility of Small Organic Molecules, *J. Am. Chem. Soc.* **1989**, *111*, 8346-8350.
- (20) Braun, J.; Koecher, M.; Schlabach, M.; Wehrle, B.; Limbach, H.-H.; Vogel, E. Nmr Study of the Tautomerism of Porphyrin Including the Kinetic HH/HD/DD Isotope Effects in the Liquid and the Solid State, *J. Am. Chem. Soc.* **1994**, *116*, 6593-6604.
- (21) Pike, S. D.; Chadwick, F. M.; Rees, N. H.; Scott, M. P.; Weller, A. S.; Krämer, T.; Macgregor, S. A. Solid-State Synthesis and Characterization of  $\sigma$ -Alkane Complexes,  $[\text{Rh}(\text{L}_2)(\eta^2, \eta^2-$

- C<sub>7</sub>H<sub>12</sub>][BAR<sup>F</sup><sub>4</sub>] (L<sub>2</sub> = Bidentate Chelating Phosphine), *J. Am. Chem. Soc.* **2015**, *137*, 820-833.
- (22) Chadwick, F. M.; McKay, A. I.; Martinez-Martinez, A. J.; Rees, N. H.; Krämer, T.; Macgregor, S. A.; Weller, A. S. Solid-State Molecular Organometallic Chemistry. Single-Crystal to Single-Crystal Reactivity and Catalysis with Light Hydrocarbon Substrates, *Chem. Sci.* **2017**, *8*, 6014-6029.
- (23) See Supporting Materials
- (24) Wilson, A. D.; Miller, A. J. M.; DuBois, D. L.; Labinger, J. A.; Bercaw, J. E. Thermodynamic Studies of [H<sub>2</sub>Rh(Diphosphine)<sub>2</sub>]<sup>+</sup> and [HRh(Diphosphine)<sub>2</sub>(CH<sub>3</sub>CN)]<sup>2+</sup> Complexes in Acetonitrile, *Inorg. Chem.* **2010**, *49*, 3918-3926.
- (25) Martínez-Martínez, A. J.; Royle, C. G.; Furfari, S. K.; Suriye, K.; Weller, A. S. Solid-State Molecular Organometallic Catalysis in Gas/Solid Flow (Flow-SMOM) as Demonstrated by Efficient Room Temperature and Pressure 1-Butene Isomerization, *ACS Catal.* **2020**, *10*, 1984-1992.
- (26) Chadwick, F. M.; Olliff, N.; Weller, A. S. A Convenient Route to a Norbornadiene Adduct of Iridium with Chelating Phosphines, [Ir(R<sub>2</sub>PCH<sub>2</sub>CH<sub>2</sub>PR<sub>2</sub>)(NBD)][BAR<sup>F</sup><sub>4</sub>] and a Comparison of Reactivity with H<sub>2</sub> in Solution and the Solid-State, *J. Organomet. Chem.* **2016**, *812*, 268-271.
- (27) Bianchini, C.; Farnetti, E.; Graziani, M.; Kaspar, J.; Vizza, F. Molecular Solid-State Organometallic Chemistry of Tripodal (Polyphosphine)Metal Complexes. Catalytic Hydrogenation of Ethylene at Iridium, *J. Am. Chem. Soc.* **1993**, *115*, 1753-1759.
- (28) The larger crystals used for single-crystal studies result in a slower solid/gas reaction with D<sub>2</sub>. The composition determined by x-ray diffraction after 40 minutes is thus more reflective of the finely powdered sample after 20 mins. See Supporting Materials.
- (29) Furfari, S. K.; Tegner, B. E.; Burnage, A. L.; Doyle, L. R.; Bukvic, A. J.; Macgregor, S. A.; Weller, A. S. Selectivity of Rh...H-C Binding in a σ-Alkane Complex Controlled by the Secondary Microenvironment in the Solid State, *Chem. Eur. J.* **2021**, *27*, 3177-3183.
- (30) Algarra, A. G.; Burnage, A. L.; Iannuzzi, M.; Krämer, T.; Macgregor, S. A.; Pirie, R. E. M.; Tegner, B.; Weller, A. S. Computational Studies of the Solid-State Molecular Organometallic (SMOM) Chemistry of Rh σ-Alkane Complexes *Struct. Bond* **2020**, *186*, 183-228
- (31) Pitts, A. L.; Wriglesworth, A.; Sun, X.-Z.; Calladine, J. A.; Zarić, S. D.; George, M. W.; Hall, M. B. Carbon-Hydrogen Activation of Cycloalkanes by Cyclopentadienylcarbonylrhodium—a Lifetime Enigma, *J. Am. Chem. Soc.* **2014**, *136*, 8614-8625.
- (32) Guan, J.; Wriglesworth, A.; Sun, X. Z.; Brothers, E. N.; Zarić, S. D.; Evans, M. E.; Jones, W. D.; Towrie, M.; Hall, M. B.; George, M. W. Probing the Carbon-Hydrogen Activation of Alkanes Following Photolysis of Tp<sup>+</sup>Rh(CNR)(Carbodiimide): A Computational and Time-Resolved Infrared Spectroscopic Study, *J. Am. Chem. Soc.* **2018**, *140*, 1842-1854.
- (33) Zhou, X.; Malakar, S.; Zhou, T.; Murugesan, S.; Huang, C.; Emge, T. J.; Krogh-Jespersen, K.; Goldman, A. S. Catalytic Alkane Transfer Dehydrogenation by PSP-Pincer-Ligated Ruthenium. Deactivation of an Extremely Reactive Fragment by Formation of Allyl Hydride Complexes, *ACS Catal.* **2019**, *9*, 4072-4083.
- (34) Bernskoetter, W. H.; Schauer, C. K.; Goldberg, K. I.; Brookhart, M. Characterization of a Rhodium(I) σ-Methane Complex in Solution, *Science* **2009**, *326*, 553.
- (35) Geftakis, S.; Ball, G. E. Direct Observation of a Transition Metal Alkane Complex, CpRe(CO)<sub>2</sub>(Cyclopentane), Using NMR Spectroscopy, *J. Am. Chem. Soc.* **1998**, *120*, 9953-9954.
- (36) Following H<sub>2</sub> or D<sub>2</sub> addition by <sup>31</sup>P{<sup>1</sup>H} NMR spectroscopy in d<sub>6</sub>-acetone solution showed that [1-COD][BAR<sup>F</sup><sub>4</sub>] was consumed at a very similar rate for both.
- (37) Hulbert, S. F. Models for Solid-State Reactions in Powdered Compacts: A Review, *J. Br. Ceram. Soc.* **1969**, *6*, 11-20.
- (38) Finney, E. E.; Finke, R. G. Is There a Minimal Chemical Mechanism Underlying Classical Avrami-Erofe'ev Treatments of Phase-Transformation Kinetic Data?, *Chem. Mat.* **2009**, *21*, 4692-4705.
- (39) Khawam, A.; Flanagan, D. R. Solid-State Kinetic Models: Basics and Mathematical Fundamentals, *J. Phys. Chem. B* **2006**, *110*, 17315-17328.
- (40) Hatcher, L. E.; Skelton, J. M.; Warren, M. R.; Stubbs, C.; da Silva, E. L.; Raithby, P. R. Monitoring Photo-Induced Population Dynamics in Metastable Linkage Isomer Crystals: A Crystallographic Kinetic Study of [Pd(Bu<sub>4</sub>Dien)NO<sub>2</sub>][BPh<sub>4</sub>], *Phys. Chem. Chem. Phys.* **2018**, *20*, 5874-5886.
- (41) Jarvis, A. G.; Sparkes, H. A.; Tallentire, S. E.; Hatcher, L. E.; Warren, M. R.; Raithby, P. R.; Allan, D. R.; Whitwood, A. C.; Cockett, M. C. R.; Duckett, S. B. et al. Photochemical-Mediated Solid-State [2+2]-Cycloaddition Reactions of an Unsymmetrical Dibenzyldiene Acetone (Monothiophos-DBA), *CrystEngComm* **2012**, *14*, 5564-5571.
- (42) Benedict, J. B.; Coppens, P. Kinetics of the Single-Crystal to Single-Crystal Two-Photon Photodimerization of α-Trans-Cinnamic Acid to α-Truxillic Acid, *J. Phys. Chem. A* **2009**, *113*, 3116-3120.
- (43) Xing, Y.; Cai, J.; Li, L.; Yang, M.; Zhao, X. An Exceptional Kinetic Quantum Sieving Separation Effect of Hydrogen Isotopes on Commercially Available Carbon Molecular Sieves, *Phys. Chem. Chem. Phys.* **2014**, *16*, 15800-15805.
- (44) Heller, D.; De Vries, A. H.; De Vries, J. G. In *The Handbook of Homogeneous Hydrogenation*; Wiley-VCH: Weinheim, 2007.
- (45) Bukvic, A. J.; Crivoi, D. G.; Garwood, H. G.; McKay, A. I.; Chen, T. T. D.; Martínez-Martínez, A. J.; Weller, A. S. Tolerant to Air σ-Alkane Complexes by Surface Modification of Single Crystalline Solid-State Molecular Organometallics Using Vapour-Phase Cationic Polymerisation: SMOM@Polymer, *Chem. Commun.* **2020**, *56*, 4328-4331.
- (46) Halasz, I. Single-Crystal-to-Single-Crystal Reactivity: Gray, Rather Than Black or White, *Cryst. Growth Des.* **2010**, *10*, 2817-2823.
- (47) Perutz, R. N.; Sabo-Etienne, S. The σ-Cam Mechanism: Σ Complexes as the Basis of σ-Bond Metathesis at Late-Transition-Metal Centers, *Angew. Chem. Int. Ed.* **2007**, *46*, 2578-2592.
- (48) Perutz, R. N.; Sabo-Etienne, S.; Weller, A. S. Metathesis by Partner Interchange in σ-Bond Ligands: Expanding Applications of the Σ-Cam Mechanism, *Angew. Chem. Int. Ed.* **2022**, in the press doi.org/10.1002/anie.202111462.
- (49) Bézier, D.; Guan, C.; Krogh-Jespersen, K.; Goldman, A. S.; Brookhart, M. Experimental and Computational Study of Alkane Dehydrogenation Catalyzed by a Carbazolidine-Based Rhodium Pnp Pincer Complex, *Chem. Sci.* **2016**, *7*, 2579-2586.
- (50) Simple thermodynamic considerations leads to a stabilization of 15 kJmol<sup>-1</sup> for each H/D exchange [D-D, 443; C-H, 413; H-D, 439; C-D, 432 kJmol<sup>-1</sup>]
- (51) Howarth, O. W.; McAteer, C. H.; Moore, P.; Morris, G. E. Reactions of Dienes with the Ion [Ir(PPh<sub>3</sub>)<sub>2</sub>(OCMe<sub>2</sub>)<sub>2</sub>H<sub>2</sub>]<sup>+</sup>: A Kinetic and Mechanistic Study of Complex Formation and Diene Hydrogenation, *Journal of the Chemical Society, Dalton Trans.* **1984**, 1171-1180.

## Table of Contents

